Supplement of

Long-term observations of cloud condensation nuclei in the Amazon rain forest – Part 2: Variability and characteristic differences under near-pristine, biomass burning, and long-range transport conditions

Mira L. Pöhlker et al.

Correspondence to: Mira L. Pöhlker (m.pohlker@mpic.de) and C. Pöhlker (c.pohlker@mpic.de)

This file includes:

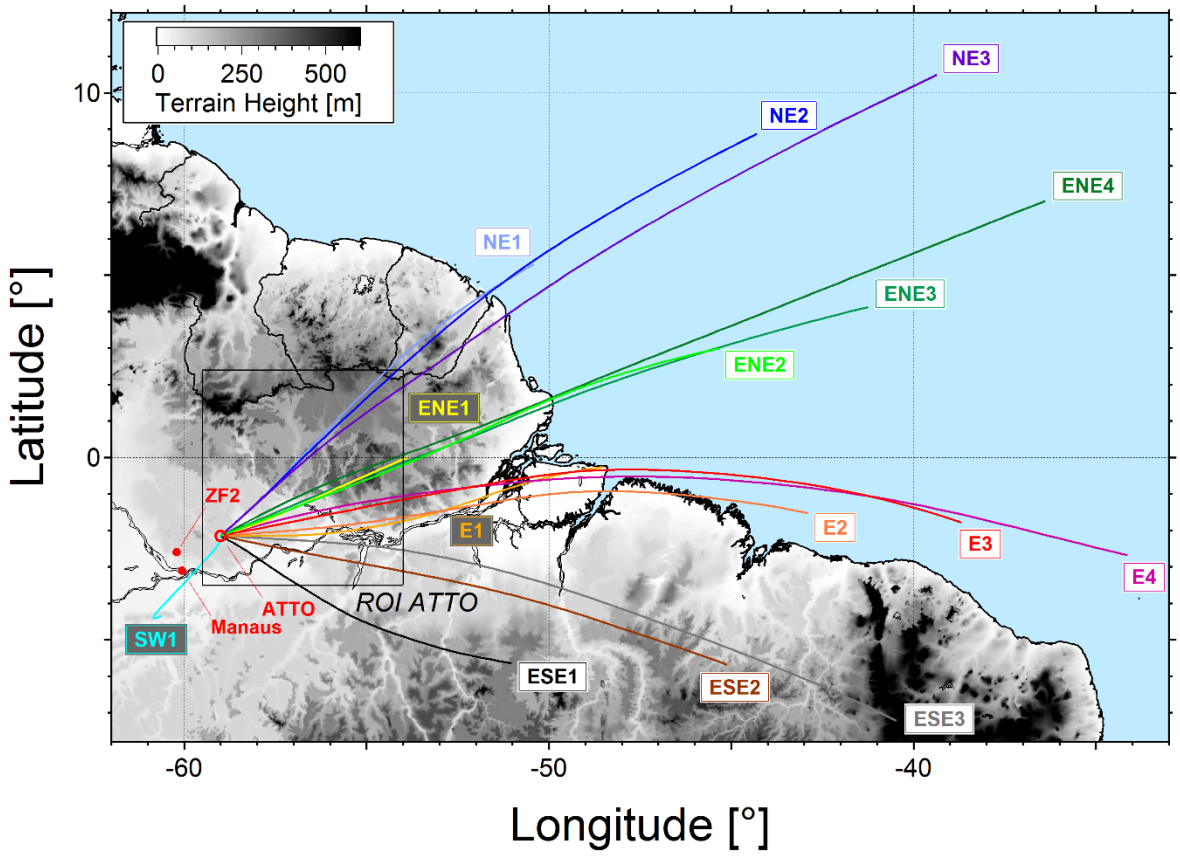

Figure S1. Map of northeast Amazon Basin with 15 final clusters from systematic BT cluster analysis based on multi-year BT data (for details see C. Pöhlker et al., 2017). The BT clusters show that air masses arrive at the ATTO site almost exclusively from northeastern to southeastern directions. Five major wind directions can be discriminated: (i) Northeastern clusters NE1, NE2, and NE3; (ii) east-northeastern clusters ENE1, ENE2, ENE3, and ENE4; (iii) eastern clusters E1, E2, E3, and E4; (iv) east-southeastern clusters ESE1, ESE2, and ESE3 and (iv) one southwestern cluster SW1. Topographic map is represented by grey scale, which is capped at 600 m. Highlighted area represents region of interest ROI_{ATTO}. Figure adapted from C. Pöhlker et al. (2017).

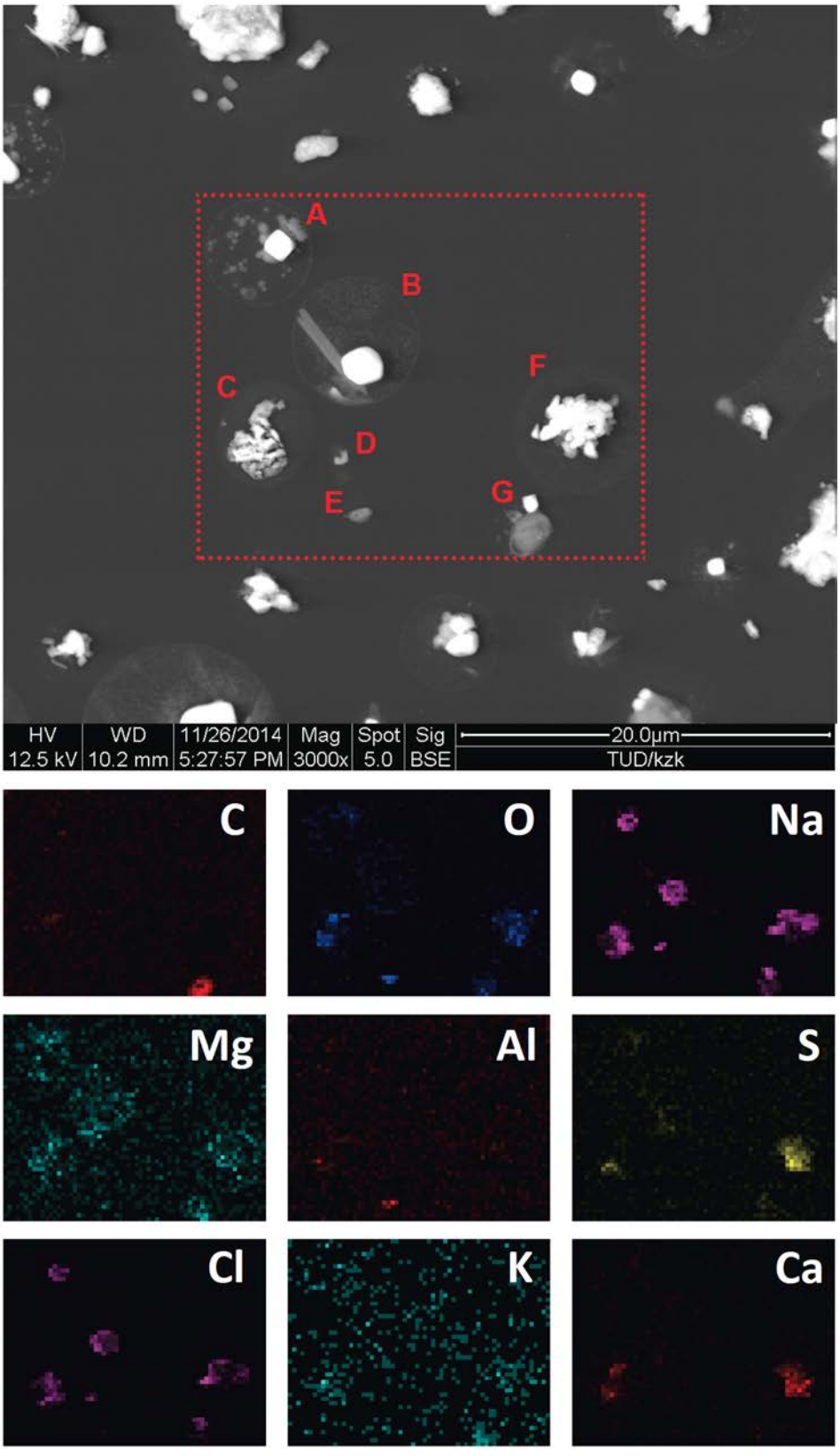

Figure S2. SEM images and EDX maps for selected aerosol sample showing typical appearance of LRT aerosol population at the ATTO site. Sample shows processed and internally mixed sea spray and dust particles. The results are based on an aerosol sample, collected on 15th Feb 2014 during LRT event

2014_2 according to Moran-Zuloaga et al. (2017), which is comparable (i.e., transport patterns, physicochemical properties recorded by online measurements) to the event discussed as LRT case study in the present work. The particles A, B, and D resemble sea spray particles with a (large) cubic crystal of NaCl as well as weaker signals in Mg, O, and S (likely as $MgSO_4$). Morphologically, the particles show similarities to examples of aged sea-salt particles in previous studies (e.g., Laskin et al., 2012). The needle-like structure in particle B could be a $CaSO_4$ crystal that appears to be too 'thin' to give a clear signal in the EDX maps. The particles C and F also show a strong NaCl signal. In addition, they reveal strong signals in S, O, and Ca. These particles resemble $CaCO_3$ particles from the Saharan dust plume, in which the CO_3^{2-} anion was (partly) replaced by SO_4^{2-} in the course of atmospheric processing. Similar particles have been described in Laskin et al. (2005). Upon processing, a certain amount of NaCl appears to be mixed in most particles. Particle G comprises a NaCl crystal that is attached to PBAP-like particle (based on morphology and strong C signal). Particle E shows signals in Al and O, which fit to an alumosilicate particle.

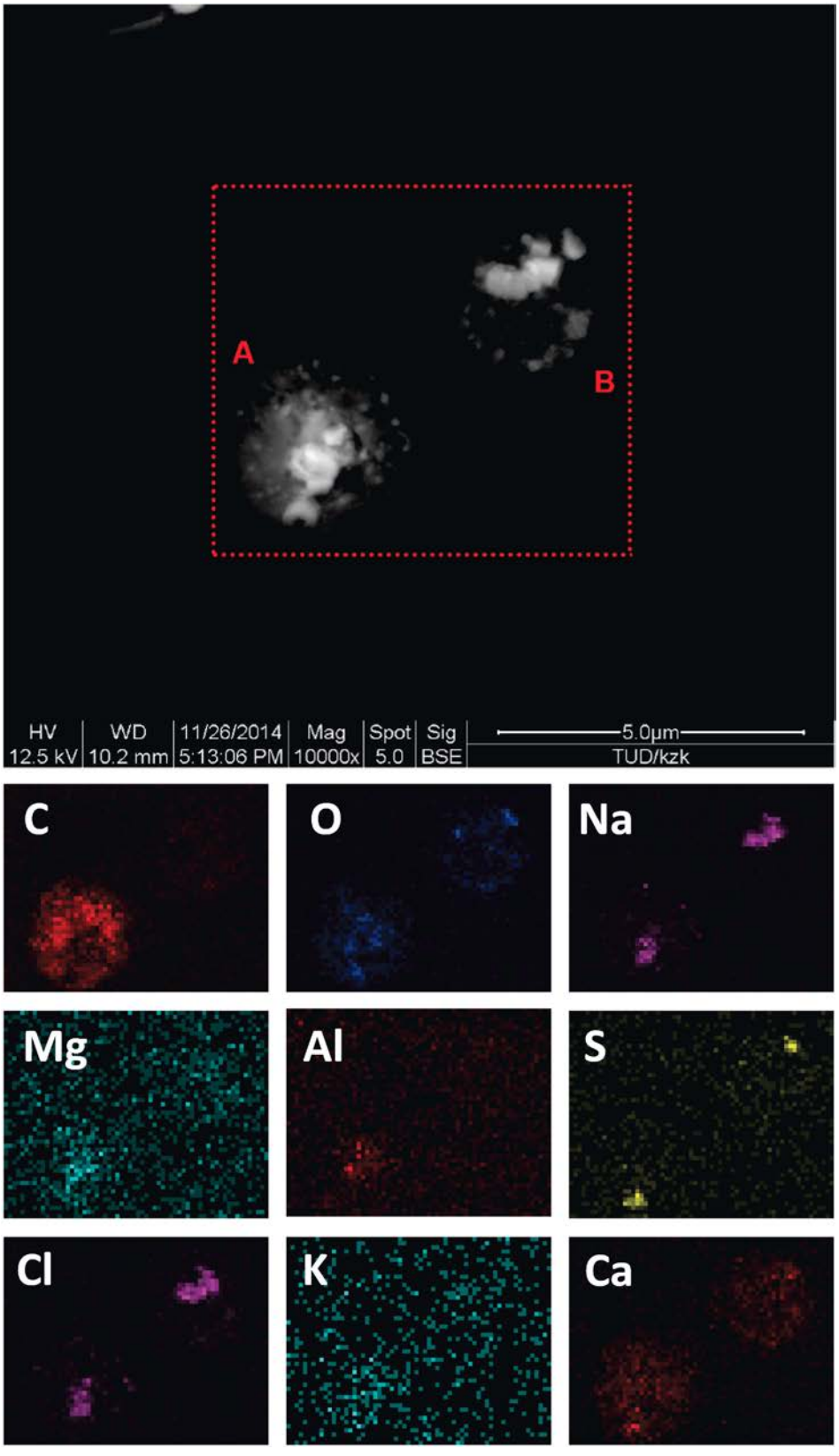

Figure S3. SEM images and EDX maps for selected aerosol sample showing a further example of the typical appearance of LRT aerosol population at the ATTO site. Sample shows processed and internally mixed sea spray and dust particles. For further relevant details, refer to caption on Fig. S2.

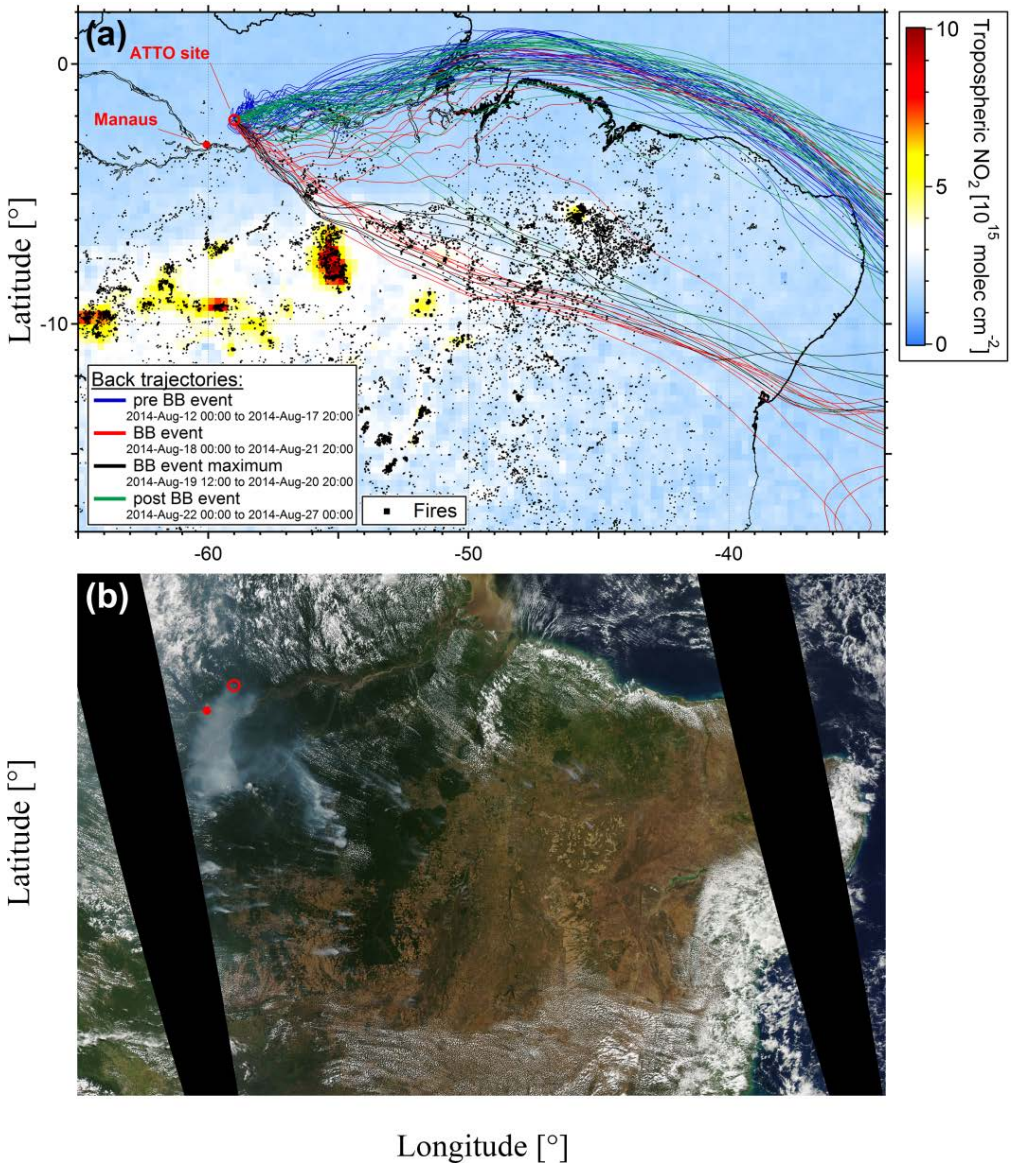

Figure S4. Composite maps illustrating origin of strong biomass burning (BB) plume that affected the ATTO site during BB case study period (17 to 23 Aug 2014). (**a**) Map combines BT ensembles for selected periods (HYSPLIT, NOAA-ARL, GDAS1, start height 200 m, BTs started every 4 h, Draxler and Hess, 1998) with satellite products for active fire counts (MODIS active fire detection extracted from MCD14ML distributed by NASA FIRMS**,** Justice et al. 2011) and NO_2 atmospheric column (OMI/Aura NO_2 Cloud-Screened Total and Tropospheric Column Daily L3 Global 0.25deg) during same period. BTs are color-coded for characteristic periods before, during, and after biomass burning event. BTs for pollution 'peak' at ATTO are color-coded as "BB event maximum". Map indicates that the BTs' main track temporarily swings from 'coastal path' to 'inland path' and back. Inland BTs intersect areas with strong fire activity, as visible in fire counts as well as in NO_2 map (i.e., 7° S, 55° W). The most intense fires are located along the highway BR-163, which is known to be a hotspot of recent deforestation activities (for details, see C. Pöhlker et al., 2017). (**b**) MODIS corrected reflectance image (taken during Aqua overflight on 19 August 2014 1700UT) confirms that major fires at about 7° S and 55° W have emitted clearly visible smoke plume that travels north-westwards and impacts the ATTO site.

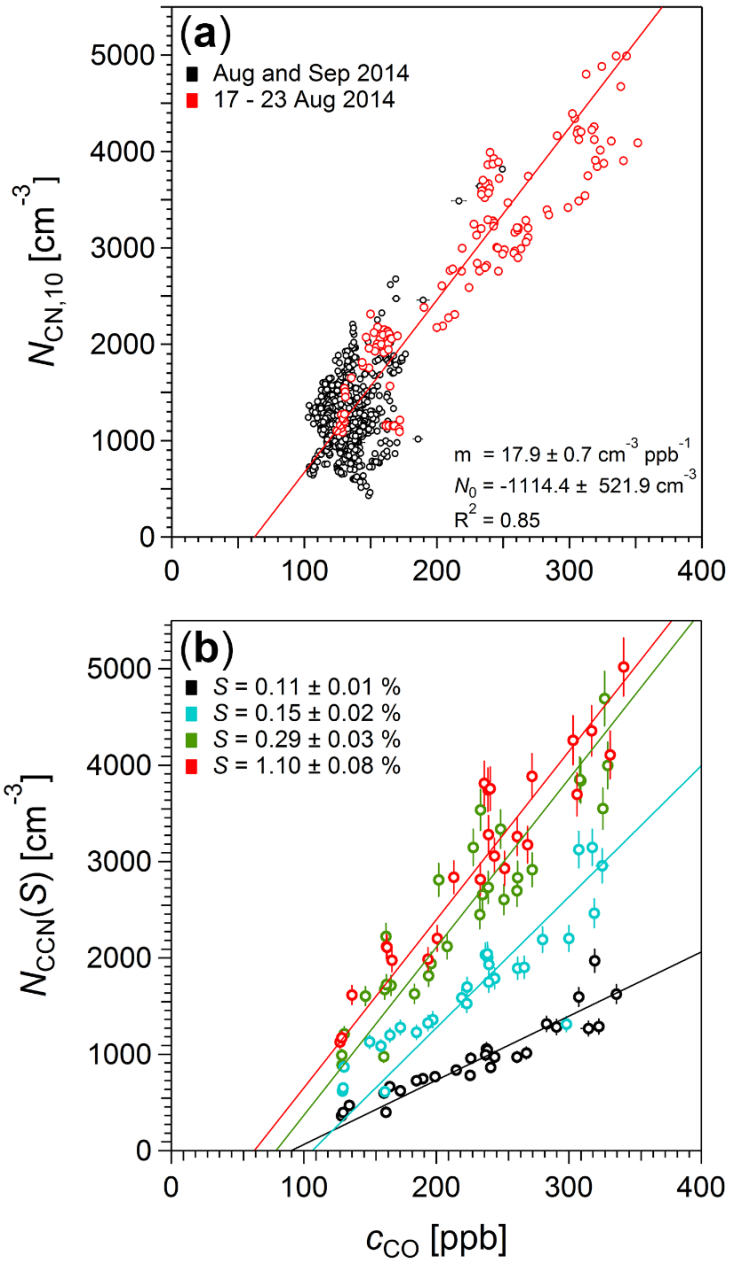

Figure S5. Scatter plots of total aerosol concentration $N_{CN,10}$ and CO mixing ratio c_{CO} (hourly average values) with bivariate regression fit in (**a**) and scatter plot of CCN concentrations $N_{CCN}(S)$ and CO mixing ratio c_{CO} for four selected S with bivariate regression fit in (**b**). Data in both cases covers peak period of the biomass burning case study *BB* (see Fig. 4). Error bars show standard errors.

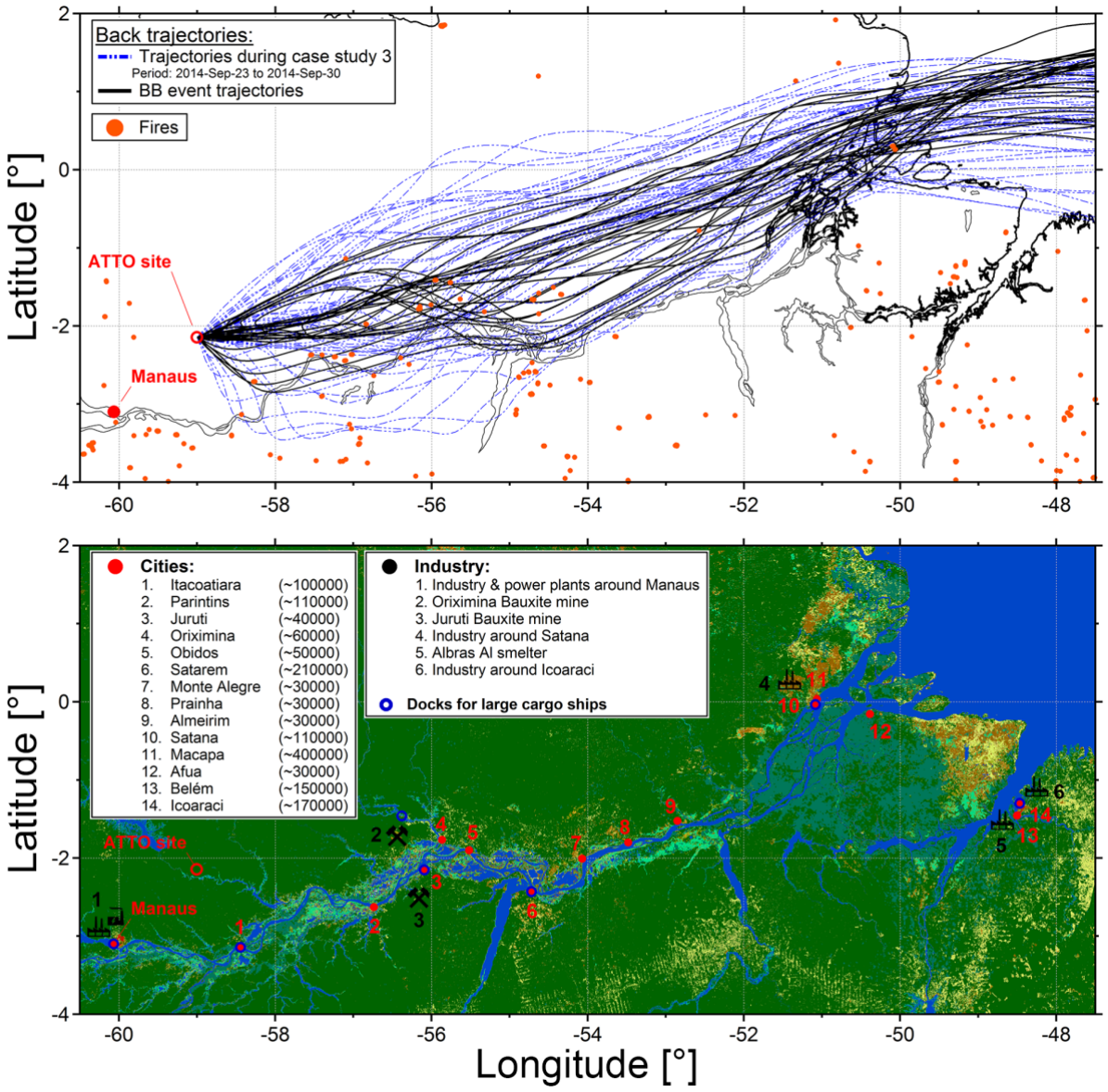

Figure S6. Composite maps illustrating conditions during *MixPol* case study (23 to 30 September 2014). Upper map combines back trajectories ensemble for selected periods (HYSPLIT, NOAA-ARL, GDAS1, start height 200 m, trajectories started every 4 h) (Draxler and Hess, 1998) with satellite products for active fire counts (MODIS active fire detection extracted from MCD14ML distributed by NASA FIRMS**)** (Justice et al., 2011) during same period. Blue trajectories represent ensemble during entire *MixPol* period. Black trajectories highlight episodes with can be attributed to biomass burning plumes (24 Sep 2014 2200UT – 26 Sep 0800UT, 27 Sep 0000UT – 27 Sep 0600UT, 29 Sep 0000UT – 29 Sep 1000UT). Main trajectory track follows westerly direction and passes several (smaller fires) along Amazon River. Lower map shows globcover 2009 data (Arino et al., 2008) and larger cities (population given in parenthesis) as well as larger industrial infrastructure along the Amazon River.

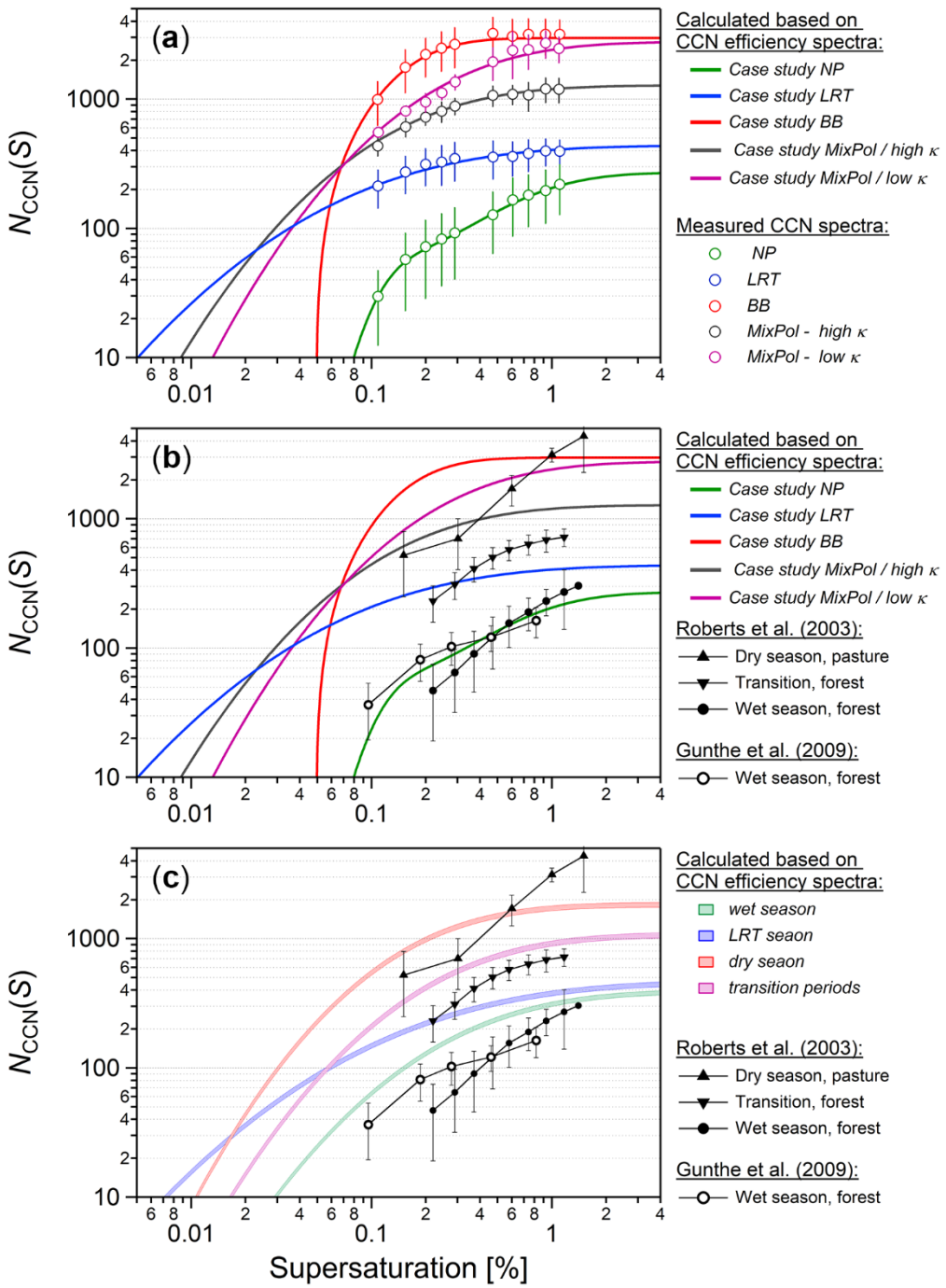

Figure S7. Comparison of CCN spectra. (**a**) Lines represent CCN spectra for case studies as defined in present part 2 paper. CCN spectra were obtained from multiplication of CCN efficiency spectra with average aerosol number concentrations for corresponding case studies. Markers represent measured average CCN concentrations for case study periods. Error bars at markers represent one std. Good agreement of CCN spectra and markers underlines reliability of CCN efficiency spectra in representation of CCN population. (**b**) Lines represent average CCN spectra for case study periods. Black markers shows CCN spectra from Amazon region as observed and reported by Roberts et al. (2003) based on several weeks of measurement data during the LBA-EUSTACH campaign in 1999 and Gunthe et al. (2009) based on several weeks of measurement data during the AMAZE-08 campaign in 2008. (**c**) Lines represent average CCN spectra for different seasons as reported in part 1 of this study (Pöhlker et al. 2016). Black markers shows CCN spectra as observed and reported by Roberts et al. (2003) and Gunthe et al. (2009).

Table S1. Excess $N_{CCN}(S)$ to excess c_{CO} ratios $\Delta N_{CCN}(S)/\Delta c_{CO}$ for the individual S levels during peak period of the biomass burning event in case study BB (17 - 23 August 2014). Ratios $\Delta N_{CCN}(S)/\Delta c_{CO}$ were obtained from bivariate regression fits (see Fig. S5b).

S **[%]**	**Δ $N_{CCN}(S)$ / ΔCO** **[cm^{-3} ppb^{-1}]**	***N*** **[cm^{-3}]**	R^2
0.11±0.01	6.7±0.5	-603 ±125	0.86
0.15±0.02	13.6±1.4	-1447 ±354	0.68
0.20±0.02	14.3±0.8	-1128 ±208	0.90
0.24±0.03	16.8±1.0	-1460 ±261	0.86
0.29±0.03	17.4±1.3	-1378 ±296	0.83
0.47±0.04	20.1±1.7	-1675 ±425	0.84
0.61±0.06	17.9±1.3	-1206 ±332	0.88
0.74±0.08	16.5±1.3	-933 ±329	0.88
0.92±0.11	18.1±1.4	-1265 ±355	0.85
1.10±0.08	17.5±1.3	-1096 ±328	0.87

Data Tables

(to be added in the course of revision)

References

Arino, O., Bicheron, P., Achard, F., Latham, J., Witt, R., and Weber, J.-L.: GLOBCOVER The most detailed portrait of Earth, Esa Bulletin-European Space Agency, 24-31, 2008.

Draxler, R. R., and Hess, G. D.: An overview of the HYSPLIT_4 modelling system for trajectories, dispersion and deposition, Australian Meteorological Magazine, 47, 295-308, 1998.

Gunthe, S. S., King, S. M., Rose, D., Chen, Q., Roldin, P., Farmer, D. K., Jimenez, J. L., Artaxo, P., Andreae, M. O., Martin, S. T., and Poschl, U.: Cloud condensation nuclei in pristine tropical rainforest air of Amazonia: size-resolved measurements and modeling of atmospheric aerosol composition and CCN activity, Atmospheric Chemistry and Physics, 9, 7551-7575, 2009.

Justice, C., Giglio, L., Roy, D., Boschetti, L., Csiszar, I., Davies, D., Korontzi, S., Schroeder, W., O'Neal, K., and Morisette, J.: MODIS-Derived Global Fire Products, in: Land Remote Sensing and Global Environmental Change, edited by: Ramachandran, B., Justice, C. O., and Abrams, M. J., Remote Sensing and Digital Image Processing, Springer New York, 661-679, 2011.

Laskin, A., Iedema, M. J., Ichkovich, A., Graber, E. R., Taraniuk, I., and Rudich, Y.: Direct observation of completely processed calcium carbonate dust particles, Faraday Discuss., 130, 453-468, 10.1039/b417366j, 2005.

Laskin, A., Moffet, R. C., Gilles, M. K., Fast, J. D., Zaveri, R. A., Wang, B., Nigge, P., and Shutthanandan, J.: Tropospheric chemistry of internally mixed sea salt and organic particles: Surprising reactivity of NaCl with weak organic acids, Journal of Geophysical Research-Atmospheres, 117, 10.1029/2012jd017743, 2012.

Moran-Zuloaga, D., Ditas, F., Walter, D., Araùjo, A., Brito, J., Carbone, S., Chi, X., Hrabe de Angelis, I., Lavric, J. V., Ming, J., Pöhlker, M. L., Ruckteschler, N., Saturno, J., Wang, Y., Wang, Q., Weber, B., Wolff, S., Artaxo, P., Andreae, M. O., and Pöhlker, C.: Coarse mode aerosols in the Amazon rain forest – A multi-year study on the frequent advection of African dust plumes Atmos. Chem. Phys., 2017.

Pöhlker, C., Walter, D., Paulsen, H., Könemann, T., Moran-Zuloaga, D., Brito, J., Carbone, S., Degrendele, C., Després, V. R., Ditas, F., Holanda, B. A., Lammel, G., Lavrič, J. V., Jing, M., Pickersgill, D., Pöhlker, M. L., Rodríguez-Caballero, E., Ruckteschler, N., Saturno, J., Sörgel, M., Wang, Q., Weber, B., Wolff, S., Artaxo, P., Pöschl, U., and Andreae, M. O.: Systematic backward trajectory and land cover analyses within the footprint of the remote ATTO site in the central Amazon Basin Atmos. Chem. Phys., to be submitted, 2017.

Roberts, G. C., Nenes, A., Seinfeld, J. H., and Andreae, M. O.: Impact of biomass burning on cloud properties in the Amazon Basin, Journal of Geophysical Research-Atmospheres, 108, 10.1029/2001jd000985, 2003.